



# Manufacturer calibrations of GPS transmit antenna phase patterns: a critical review

Oliver Montenbruck<sup>1</sup> · Peter Steigenberger<sup>1</sup> · Torsten Mayer-Gürr<sup>2</sup>

Received: 9 September 2023 / Accepted: 18 November 2023 / Published online: 27 December 2023  
© The Author(s) 2023

## Abstract

Over the past decade, the Global Positioning System has released pre-flight calibrations for the transmit antennas of the Block IIR/IIR-M, Block IIF, and GPS III satellites that make up the current GPS constellation. Frequency-specific phase variations (PHVs) provided as part of these data sets are of key interest for an accurate and consistent modeling of GNSS carrier phase observations in precise point positioning applications as well as orbit and clock offset determination of the GPS satellites themselves. For proper utilization of the manufacturer calibrations, complementary information on the phase center offset (PCO) from the spacecraft center-of-mass is required. We describe necessary processing steps for converting the raw phase calibrations of Lockheed Martin and Boeing into a representation compatible with antenna models of the International GNSS Service (IGS), and provide a detailed discussion of inherent assumptions for combining PHVs and PCOs from different sources. Comparison with estimated antenna data from globally distributed monitoring stations shows good consistency of PHVs and suggests the use of manufacturer-calibrated, azimuth-dependent patterns in future releases of the IGS antenna model. In terms of PCOs, the new Block IIF calibrations exhibit a systematic bias of about 12 cm from PCOs estimates based on the IGS20 reference frame. This value closely matches the bias observed for manufacturer calibrations of GPS III and Galileo satellites, and suggests a careful review of the contribution that GNSS can make to the scale definition of the International Terrestrial Reference Frame (ITRF).

**Keywords** GPS · Transmit antennas · Phase patterns · PCO · ITRF · Spaceborne GPS

## 1 Introduction

In the absence of comprehensive and consistent pre-flight calibrations, the processing of GNSS observations has traditionally relied on empirical transmit antenna phase variations (PHVs) and phase center offsets (PCOs) from the center-of-mass (COM). These were adjusted by the International GNSS Service (IGS, Johnston et al. 2017) from observations of a

global station network and incorporated into conventional antenna models for use with IGS orbit and clock products. Since the radial component of the PCO is strongly correlated with the station height (Zhu et al. 2003), updated antenna models have been derived when adopting a new release of the International Terrestrial Reference Frame (ITRF) for GNSS data processing (Schmid et al. 2016; Reischung and Schmid 2016; Villiger 2022).

Recognizing the benefit of independent antenna calibrations for precise GNSS processing and their potential contribution to a GNSS-based definition of the ITRF scale, consistent sets of PCO/PHV data from manufacturer calibrations were released for satellites of the European Galileo system in 2016 (EUSPA 2022) and the Quasi-Zenith Satellite System in 2017 (Cabinet Office 2023), and subsequently incorporated into the IGS antenna model. Even earlier, phase pattern calibrations of the Block IIR and IIR-M transmit antennas were released by the Global Positioning System (GPS; Marquis 2014). However, the data covered only a subset of the then active GPS constellation and their use was hampered by the

---

✉ Oliver Montenbruck  
oliver.montenbruck@dlr.de

Peter Steigenberger  
peter.steigenberger@dlr.de

Torsten Mayer-Gürr  
mayer-guerr@tugraz.at

<sup>1</sup> Deutsches Zentrum für Luft- und Raumfahrt, German Space Operations Center Münchener Straße 20, 82234 Weßling, Germany

<sup>2</sup> Graz University of Technology, Institute of Geodesy, Steyregasse 30/III, 8010 Graz, Austria

lack of associated phase center locations. As such, the IGS continued to rely on estimated GPS antenna phase centers and patterns for many years, and deferred use of the respective manufacturer calibrations for several years. The only manufacturer-based GPS antenna parameters in the current IGS model so far are the PCOs of the GPS III satellites (Lockheed Martin 2021). These have been gradually added to the model since the launch of the first GPS III satellite in 2019.

This study presents a systematic review of pre-flight calibrations for the phase patterns of the GPS IIR, IIF, and III transmit antennas, and discusses their prospects and limitations for use in precise GPS processing. The currently available data sets released by Lockheed Martin and Boeing as well as auxiliary information from the National Geospatial-Intelligence Agency are introduced in Sect. 2 along with a discussion of necessary assumptions for their interpretation and processing. Section 3 discusses the conceptual definition of an antenna phase center and highlights the consequences of different grid types and sampling points when estimating the phase center location from measured phase variations. A comparison of phase patterns derived from the manufacturer calibrations with observed phase patterns is presented in Sect. 4 including a discussion of phase variations beyond the Earth coverage region that is of interest for spaceborne GPS tracking. Furthermore, phase center locations derived from the manufacturer calibrations are compared with currently adopted values of the IGS antenna model. Section 5 finally presents a new antenna model consistent with the IGS20 reference frame, which combines phase variations from the manufacturer calibrations with observed phase center offsets and may serve as a prototype for a future refinement of the IGS antenna model.

## 2 Calibration data sets

The presently available set of antenna calibrations comprises phase pattern information for the Block IIR/IIR-M and GPS III satellites built by Lockheed Martin as well as the Block IIF satellites of Boeing. Complementary satellite antenna offsets have been published by Lockheed Martin for the GPS III satellites and by the National Geospatial-Intelligence Agency (NGA 2014, 2020) for the operational satellites at the times of publication.

### 2.1 Lockheed Martin

Block IIR and IIR-M phase pattern data from pre-flight measurements for the L1 and L2 frequency were first released in Marquis (2014) with clarifications/corrections of the calibration reference frame provided in Marquis (2015). Within the Block IIR generation, two different types of L-band antenna panels are employed. While eight out of twelve IIR satel-

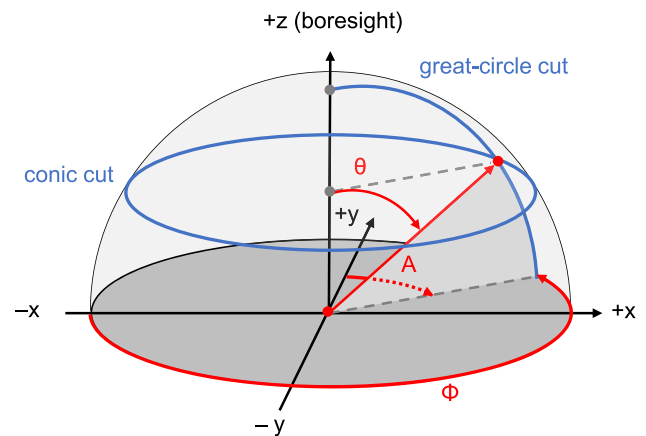


**Fig. 1** Illustration of angles used in the measurement and description of antenna phase patterns, including the off-boresight angle  $\theta$ , the in-plane angle  $\Phi$ , and the azimuth angle  $A$ . Axes are labeled in accordance with IGS conventions (Montenbruck et al. 2015). Depending on the spacecraft manufacturer, the in-plane angle is measured from the  $-x$  axis (Lockheed Martin) or the  $+x$  axis (Boeing)

lites are equipped with the legacy panel, a new and improved antenna panel developed as part of the IIR modernization program (Hartman et al. 2000) is used on the four remaining satellites (Marquis and Reigh 2015). For ease of distinction, IIR satellites with legacy and modernized panels are identified as IIR-A and IIR-B, respectively, within the IGS antenna model. The modernized panel is also used throughout the IIR-M generation, yielding highly similar gain and phase patterns for IIR-B and IIR-M satellites.

Following Marquis and Reigh (2015), the calibrations of the legacy and modernized panels were performed at two different spherical near-range test facilities of Lockheed Martin located at Valley Forge and Newtown, respectively. It remains unclear, though, whether or to what extent the calibrations are affected by technical or handling differences in the two facilities. To better represent the actual conditions in space, the L-band antenna panels under test were combined with a mock-up of the additional structural elements on the Earth pointing satellite face. This included various additional sensors and antennas, and offered a near-field environment closely matching the actual flight conditions for the L-band antenna calibration.

Irrespective of the panel type and test range, the pattern measurements for all satellites are based on meridional, great-circle cuts for in-plane angles  $\phi = 0^\circ, 10^\circ, \dots, 350^\circ$  and covering an off-boresight angle range of  $\theta = [-90^\circ, +90^\circ]$  at  $2^\circ$  spacing (Fig. 1). In view of the  $180^\circ$  coverage of each cut, each sampling point  $(\phi, \theta)$  coincides with a corresponding sampling point at  $(\phi \pm 180^\circ, -\theta)$ . However, with rare exceptions showing minor differences, identical phase measurements are reported for the redundant sampling points. It is therefore sufficient to consider only the positive  $\theta$  range.

A comprehensive discussion of the calibration data sets is given in Marquis and Reigh (2015) and Marquis (2016) but neither reference provides information on the location of the calibration reference point to which the individual phase measurements are referred. Dilssner et al. (2016) and Marquis (2016) both point to the fact that the measured phase data should be used in combination with NGA antenna offset values, but lack a concise description of the phase center definition that would be required for a consistent and unambiguous combination of the PHV and PCO data sets.

Following the IIR and IIR-M satellites, the latest GPS III generation was again built by Lockheed Martin, which was likewise responsible for the L-band antenna design and calibration. While not officially confirmed, the gain and phase patterns of the GPS III antenna exhibit high similarity with those of the modernized IIR/IIR-M panel, suggesting that the respective antenna type has been reused with at best minor modifications. It may be noted, though, that a second L-band antenna with a smaller number of elements has been added on GPS III, which is dedicated to the transmission of M-code signals (Thoelert et al. 2019).

Starting with the first GPS III satellite, space vehicle number SVN 74 (Lockheed Martin 2019), frequency-specific L1, L2, and L5 PCOs of the individual GPS III satellites were published by Lockheed Martin within several months after launch. As of 2023, the latest set of PCO values in Lockheed Martin (2021) covers five out of six operational satellites. It includes several updates to previously released data for the first four satellites, which generally offer an improved consistency with independent PCO estimates based on global monitoring networks (Steigenberger et al. 2020; Dilssner et al. 2023).

Phase pattern information for the first five GPS III satellites is provided in Fisher (2022). The data comprise measured phase variations on the L1, L2, and L5 frequency. The phase pattern measurements are based on great-circle cuts with the same grid and redundancy as the earlier IIR/IIR-M calibrations, but again lack a description of the calibration reference point and its relation to the spacecraft center-of-mass. Similar to the earlier satellite generation, additional assumptions need to be made for combining PCO and PHV information and for enabling a consistent use in GPS data processing.

## 2.2 Boeing

Block IIF satellites were launched in the 2010–2015 time frame and make up more than one-third of the operational GPS constellation in 2023. The recent release of IIF antenna patterns by Boeing (Igwe 2023) thus closes a major gap in the availability of manufacturer calibrations for GPS. The published data comprise two independent sets of phase calibrations obtained in conic and great-circle cuts (Fig. 1). The

conic cuts provide phase measurements for in-plane angles  $\phi = 0^\circ, 1^\circ, \dots, 359^\circ$  at  $1^\circ$  sampling and an unevenly spaced set of off-boresight angles  $\theta = 0^\circ, 2^\circ, \dots, 10^\circ, 12^\circ, 14.3^\circ, 20^\circ, 23^\circ$ . The complementary great-circle cuts cover the full range of  $\theta = [-90^\circ, +90^\circ]$  at  $1^\circ$  steps, but are limited to a sparse set of four in-plane angles at  $45^\circ$  sampling. Also, great-circle cut measurements are only given for nine out of the twelve IIF satellites (SVN 62–64 and 68–73). Given the intended use for (near-)Earth applications and the availability for all IIF spacecraft, only the conic-cut phase measurements are considered in the present work.

## 2.3 Interpretation and processing of manufacturer calibrations

In view of the partly incomplete documentation of the GPS antenna calibrations, three key assumptions have to be made for the joint processing of the published phase center and pattern data:

- NGA PCOs as given in NGA (2014, 2020) represent the values adopted up to 2021 by the 2nd Space Operations Squadron (2SOPS) for generation of the legacy broadcast navigation message for L1 users (Malys et al. 2021; NGA 2021). We assume that these values describe the location of the L1 phase centers relative to the COM, rather than that of the ionosphere-free L1/L2 combinations as assumed in the early analysis of Dilssner et al. (2016). Aside from offering the best overall consistency of IGS and manufacturer data for Block IIR/IIR-M as well as IIF satellites, the validity of this assumption is supported by the rigorous match of NGA's SVN 74 PCO with the L1 PCO value first published in Lockheed Martin (2019).
- Conceptually, the antenna phase center represents a point, relative to which the wavefront shows the smallest deviation from a sphere. Other than wide-beam receive antennas, GNSS transmit antennas are characterized by a notably focused gain pattern, and phase pattern flatness is mainly required up to the edge of Earth rather than across the entire hemisphere. As such, we assume that the manufacturer-provided PCOs relate to a phase center, which minimizes the phase variations over the Earth coverage region. More specifically, we assume that the published phase center locations are derived by minimizing the phase deviation in a least-squares sense over all measured grid points up to (and including) a maximum off-boresight angle of  $\theta_{\max} = 14^\circ$  for the Lockheed Martin phase calibrations of Block IIR/IIR-M/III antennas and up to  $\theta_{\max} = 14.3^\circ$  for Boeing's conic-cut calibrations of the Block IIF antennas.

For the Lockheed Martin calibrations, the assumption is strongly motivated by the fact that it allows to con-

**Table 1** Relative  $z$  offsets (in [m]) of phase center (PC), calibration reference point (CRP), and center-of-mass (COM) of GPS III satellites for the L1, L2, and L5 frequency

	PC <sub>est</sub> –CRP			PC <sub>LM</sub> –COM			CRP–COM+(PC <sub>LM</sub> –PC <sub>est</sub> )		
	L1	L2	L5	L1	L2	L5	L1	L2	L5
G074	–0.988	–1.498	–1.464	1.090	0.598	0.637	2.079	2.096	2.101
G075	–0.988	–1.477	–1.478	1.099	0.613	0.616	2.088	2.090	2.094
G076	–0.993	–1.472	–1.458	1.094	0.618	0.636	2.087	2.090	2.095
G077	–0.995	–1.483	–1.505	1.098	0.612	0.595	2.094	2.095	2.100
G078	–0.999	–1.505	–1.502	1.096	0.592	0.600	2.096	2.098	2.102

The frequency-specific phase centers estimated by minimization of the measured phase variations (Igwe 2023) over a  $10^\circ \times 2^\circ$  ( $A, \theta$ ) grid up to  $\theta_{\max} = 14^\circ$  are denoted by the subscript <sub>est</sub>, while the phase centers adopted in Lockheed Martin (2021) are denoted by <sub>LM</sub>

sistently reproduce the relative location of the L1, L2, and L5 phase centers of the GPS III satellites published in Lockheed Martin (2021) from the phase measurements reported in Fisher (2022). As shown in Table 1, estimated phase center offsets from the calibration reference point (CRP) yield a consistent value of 2.094 m with 6 mm standard deviation across all satellites and frequencies for the CRP–COM offset, when combined with the independently published PCO values. For Boeing, no independent confirmation is available, but the resulting L1/L2 phase centers are found to exhibit good consistency with IGS observations across the various IIF satellites, when assuming the aforementioned phase center definition.

- The Boeing phase measurements exhibit an almost linear dependency  $d\Phi/d\phi \approx -1$  of the reported phase measurement  $\Phi$  on the in-plane angle  $\phi$ , which suggests that the data are affected by the phase windup effect (Wu et al. 1993). We therefore apply a corresponding correction to the published IIF phase calibration data prior to further use. No such correction is required for the Lockheed Martin calibrations, which appear to be free of phase windup contributions.

For the subsequent analysis and applications, the phase calibration data were expressed in the ANTeNna EXchange format (ANTEX; Rothacher and Schmid 2010). Aside from formatting aspects, the ANTEX conversion includes a change of units (phase angle to range), the unwrapping of phase roll-overs, a sign change to match the definition of the ANTEX phase range correction, and, in the case of the Boeing calibrations, a phase-windup correction. Considering that the ANTEX phase patterns refer to an equidistant grid ( $A, \theta$ ) of azimuth and off-boresight angles, where  $A$  is measured clockwise from the  $y$ -axis to the  $x$ -axis (Fig. 1), the in-plane angles  $\phi$  are mapped to  $A = 90^\circ - \phi$ . For Lockheed Martin satellites, an additional  $180^\circ$  azimuth correction is applied to account for a different orientation of the Lockheed Martin body axis ( $+x$  to deep space; Marquis 2016) as compared to IGS conventions ( $+x$  to Sun-lit hemisphere; Montenbruck et al. 2015). Finally, the phase center location relative to

the calibration reference point and a possible phase bias in the calibration data are determined for each individual frequency band and used to obtain a corrected phase pattern with minimized variations over the sampling grid. Details of this process are described in Sect. 3.

### 3 Phase center estimation and correction

Considering transmit antenna contributions, carrier phase observations  $\varphi$  in precise GNSS processing are represented as the sum of the geometric range relative to an agreed-upon transmit antenna phase center and the line-of-sight dependent phase variations (Hauschild 2017). Phase center location and phase variations are treated as inseparable parts of the antenna model. Together, they enable an accurate and consistent carrier phase modeling irrespective of the conceptual phase center definition. Changes  $\Delta \mathbf{r}$  in the phase center location result in a carrier range change  $\Delta \varphi = -\mathbf{e}^T \Delta \mathbf{r}$ , where  $\mathbf{e}$  denotes the line-of-sight unit vector from the transmit antenna to the observer. The definition of phase variations is, furthermore, ambiguous with respect to additive constants  $\Delta b$  that are indistinguishable from the carrier phase ambiguities and phase biases in the observation model.

When translating phase variations between different reference point locations, the overall phase pattern correction is therefore described by

$$\Delta \varphi = -\mathbf{e}^T \Delta \mathbf{r} + \Delta b. \tag{1}$$

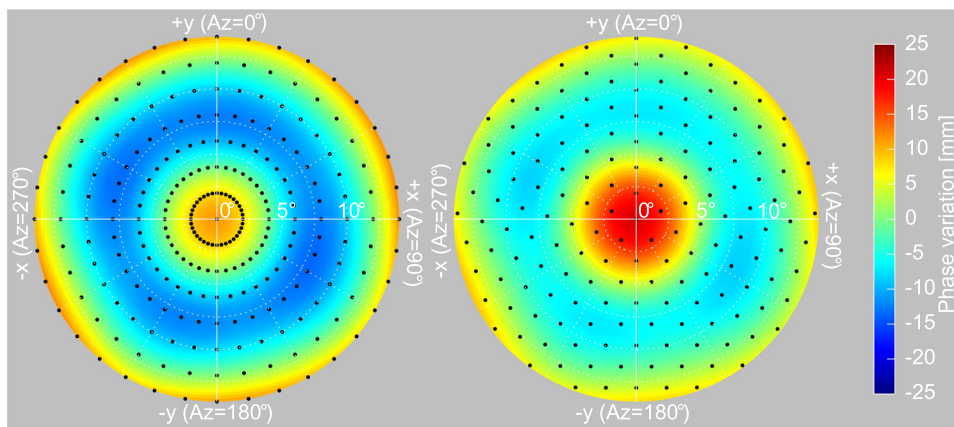
When working with Cartesian coordinates  $(x, y, z)$  of the reference point  $\mathbf{r}$  in the antenna/spacecraft frame, the alternative relation

$$\Delta \varphi = -\cos(A) \sin(\theta) \cdot \Delta x - \sin(A) \sin(\theta) \cdot \Delta y + (1 - \cos \theta) \cdot \Delta z + \Delta c \tag{2}$$

(Schmid et al. 2005; Bar-Sever et al. 2006) can be used to express the phase change as a function of changes in the four offset and bias parameters. Compared to Eq. (1), a slightly different parameterization with  $\Delta c = \Delta b - \Delta z$  is used in



**Fig. 2** Least-squares minimization of a sample L1/L2 antenna pattern (SVN 48, Block IIR-M) by phase center and bias adjustment using a regular  $10^\circ \times 2^\circ$  grid (left) and a triangular icosphere grid with  $\approx 2^\circ$  separation of neighboring vertices (right) over a  $14^\circ$  off-boresight angle range. Individual grid points are marked by black solid circles and weighted equally ( $w = 1$ )



Eq. (2), which helps to decorrelate the  $z$  offset and the bias parameter when jointly estimating these values from observations over a small off-boresight angle range.

Phase measurements provided in the manufacturer calibrations describe the variation of the measured phase relative to a calibration reference point (CRP), which remains fixed in space while the line-of-sight between the antenna under test and the receiving antenna of the calibration system is varied over the desired range of azimuth and off-boresight angles. Using, without loss of generality, the second parameterization, the offset  $\Delta \mathbf{r}_{PC-CRP} = \Delta(x, y, z)$  of the phase center (PC) from the calibration reference point may be obtained by minimizing the weighted square sum

$$J = \sum_k w_k \cdot (\varphi_{cal,k} - \Delta\varphi_k(\Delta x, \Delta y, \Delta z, \Delta c))^2 \quad (3)$$

of measured phases  $\varphi_{cal}$  and the correction  $\Delta\varphi$  over a specified set of grid points  $k$ .

At this stage, it is important to note that the estimated phase center location and bias depend crucially on the distribution of grid points adopted for the least-squares adjustment as well as the respective weighting. While minimization of the resulting phase variation is a widely agreed concept for the conceptual definition of antenna phase centers, the specific choices of grid and weighting are rarely documented in practical applications. Since antenna patterns are most often measured and documented for a rectangular grid  $(A_i, \theta_j)_{i=1, \dots, n, j=1, \dots, m}$  with a given set of azimuth and off-boresight angles, these grids offer a convenient choice for the phase pattern minimization and PCO estimation. By way of example, the relative location of the L1, L2, and L5 PCOs published by Lockheed Martin for the GPS III satellites can be reproduced by minimizing the published phase calibrations over the corresponding sampling grid up to  $\theta = 14^\circ$  (Sect. 2.3) with equal weighting of all data points. Within the IGS, GPS transmit antenna phase patterns are limited to azimuth-averaged patterns that are obtained by averaging over an equidistant grid of azimuth angles and minimization over an equidistant  $\theta$  grid up to the same limit. In both cases,

the effective number of sampling points within a given solid angle increases notably toward  $\theta = 0^\circ$  and results in a dominant contribution of phase measurements near the boresight direction.

However, the actual distribution of observations in GNSS processing is more closely represented by an isotropic distribution of sample points or, equivalently, an equal-area weighting (Montenbruck et al. 2022). When working on a rectangular  $(A, \theta)$  grid, this can be achieved by using a weight factor  $w_k = \sin \theta_k$ , which is proportional to the area on the unit sphere covered by the cell around the  $k$ -th grid point. Alternatively, triangular vertex grids may be employed, which are also known as “icospheres” or “geodesic polyhedra” (Kenner 2003). Starting from an icosahedron, polyhedra with a higher number of vertices and decreasing size of the triangular faces are constructed by consecutive division of the edges and projection of the resulting points on the unit sphere. While the triangular surfaces described by the resulting grid are not of strictly equal size, the vertices exhibit a smooth overall distribution without apparent inhomogeneities near the boresight direction. The grids are widely used in geoscience for representing, modeling, and sampling data on the spherical surface of the Earth, and have first been proposed and used for phase pattern adjustment of GNSS transmit antennas by Zehentner (2016).

For illustration, Fig. 2 shows the impact of different grids on the minimized L1/L2 phase pattern of a sample Block IIR-M satellite after adjusting the phase center and bias. In the case of the evenly-spaced  $(A, \theta)$  grid, the remaining pattern exhibits amplitudes of about  $\pm 10$  mm with a balanced variation across the considered range of off-boresight angles. Use of the icosphere grid with equal weighting ( $w = 1$ ), in contrast, leaves a pronounced peak of about 20 mm near the boresight direction, since the small number of grid points in this region contributes only moderately to the overall loss function. However, the icosphere grid yields much lower phase variations  $\varphi < 5$  mm for  $\theta \gtrsim 4^\circ$  and minimizes the squared sum of residuals similar to the equal-area weighting.

Phase center locations estimated in the two cases differ by about 40 cm in  $z$ -direction, which highlights the need for a concise definition of the estimation scheme when comparing PCOs from different sources. Nevertheless, it should be emphasized once again, that each individual set of PCOs and PHVs by itself offers a consistent and accurate description of the overall antenna pattern for GPS observation modeling. Use of a specific grid and weighting in the estimation of phase patterns thus remains a matter of convention, but requires proper attention when working with PCOs and PHVs from potentially different sources.

For best compatibility with GPS PCO/PHV models currently used within the IGS, as well as the GPS III phase center estimation concept of Lockheed Martin, we apply a rectangular ( $A, \theta$ ) grid for phase center adjustment in the processing of manufacturer calibrations. In accord with the available data sets, a  $10^\circ \times 2^\circ$  grid is used for the Block IIR/-M and GPS III satellites of Lockheed Martin, considering off-boresight angles up to and including  $\theta_{\max} = 14^\circ$ . For Block IIF satellites, on the other hand, a  $1^\circ$  azimuth sampling is applied and the off-boresight angles are sampled on a partly irregular grid of  $\theta = 0^\circ, 2^\circ, \dots, 10^\circ, 12^\circ, \text{ and } 14.3^\circ$ .

Different from the phase center adjustment, we make use of a triangular icosphere grid for the statistical characterization of individual phase patterns and for comparison of observed patterns with manufacturer data. The employed grid is constructed from an icosahedron by five consecutive bisections and offers spacings of about  $2^\circ$  between neighboring grid points. As discussed above, the icosphere grid offers a fairly isotropic distribution of sampling points, and provides a better representation of the actual distribution of GPS observations. Accordingly, phase pattern statistics based on the icosphere grid are considered to offer an improved realism and relevance for practical applications than those based on a rectangular grid.

## 4 Results and discussion

Based on the concepts discussed above, phase variations relative to a best-fit phase center have been determined from the manufacturer calibrations of the Block IIR, IIR-M, IIF, and GPS III satellites. In a first step, the resulting phase patterns are compared with observed phase patterns. Secondly, we derive frequency-specific phase center locations relative to the center-of-mass from the manufacturer calibrations and compare the results with observed PCOs based on the IGS20 reference frame.

### 4.1 Phase variations

The two-dimensional (2D) phase patterns of the GPS transmit antennas for the ionosphere-free L1/L2 combination are

illustrated in Fig. 3 using a single sample satellite of each block and antenna type. Next to the manufacturer calibrations, observed phase patterns derived for the present study by the Technical University of Graz (TUG) are shown for comparison. The patterns were obtained from three months of observations covering the period of December 2022 to March 2023. Data from all available IGS globally distributed multi-GNSS stations (approx. 380 each day) were processed with the GROOPS software (Mayer-Gürr et al. 2021) in a global parameter adjustment using an uncombined formulation of the observation model (Strasser et al. 2019) and carrier phase ambiguity fixing. Based on the associated normal equations, phase patterns for the ionosphere-free L1/L2 combination were adjusted as described in Zehentner (2016).

For a consistent comparison, all patterns were minimized based on equal weighting ( $w = 1$ ) over a rectangular grid up to off-boresight angles of  $14^\circ$ . All of the considered antenna types are made up of an outer ring of eight helix antenna elements and an inner ring of four elements, which are phase-coherently combined to achieve an approximate isoflux pattern over the surface of the Earth (Marquis 2016; Maqsood et al. 2017). This layout results in a fourfold symmetry of the phase patterns, which is clearly visible for all satellite and antenna types. Due to a  $22.5^\circ$  twist between the inner and outer antenna ring (Martzen et al. 2015), the cardinal directions of the patterns exhibit a small azimuth offset from the main body axes. As expected from the common design, GPS III patterns closely resemble those of the IIR-M satellites, while distinct characteristics are obvious for the IIR-A and IIF patterns. For the SVN 62 GPS IIF satellite, the patterns presented here show a good overall agreement with early observations discussed in Dilssner (2010).

With the given minimization conditions, roughly equal positive and negative peak values of the phase variations are obtained for the individual antenna types. However, an almost two times higher amplitude of about 13 mm is obtained for IIR-B/M and GPS III satellites as compared to IIR-A and IIF. Visual comparison of manufacturer calibrations and observed patterns in Fig. 3 shows a good overall agreement, but also reveals differences in selected details. Minor deviations from the  $90^\circ$  azimuth symmetry can be seen in all manufacturer calibrations and are mostly confirmed by the observed patterns.

For a quantitative evaluation, root-mean-square (RMS) differences for pairs of patterns were evaluated over a triangular vertex grid (cf. Figure 2, right). Subsequently, median values of the RMS differences across satellites of individual blocks were formed to characterize the properties of the various antenna types.

The scatter of phase patterns across different satellites is quantified in Table 2, which provides median RMS differences for all pairs of satellites within a block for both the manufacturer calibrations and the observed patterns of TUG.

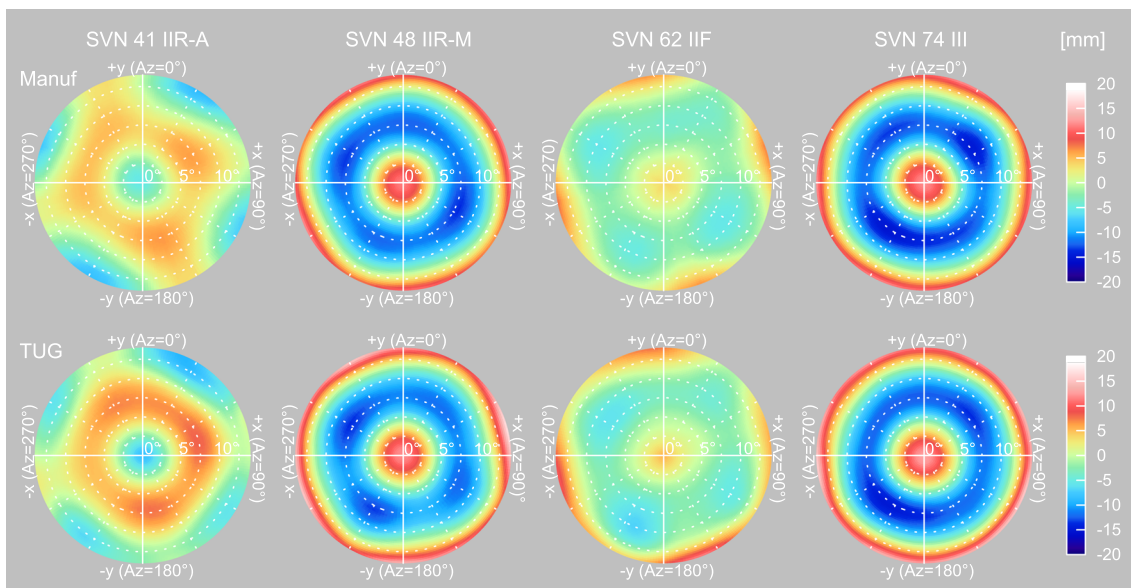


**Fig. 3** L1/L2 phase patterns of representative Block IIR, IIR-M (=IIR-B), IIF, and GPS III satellites (left to right) up to  $\theta_{max} = 14^\circ$  based on manufacturer calibrations (top) and TU Graz (bottom) estimates

**Table 2** Consistency of GPS L1/L2 phase patterns across satellites of each block for manufacturer-calibrated and observed phase patterns

Block	LMB	TUG
IIR	1.3	1.2
IIR-B/IIR-M	1.2	1.3
IIF	0.7	0.8
III	1.0	1.2

All values are given in mm and represent median values of the respective RMS differences on a triangular vertex grid for all possible pairs of satellites within the given block. LMB = Lockheed Martin/Boeing

The results demonstrate a low dispersion at the 1-mm level and thus a high repeatability of both the manufacturing process and the phase pattern determination. A particularly good overall consistency is obtained for the IIF satellites. However, an obvious anomaly may be recognized in the Boeing calibrations of three satellites (SVN 65–67), which exhibit a notable distortion near the boresight direction (Fig. 4). No such distortions show up in the observed patterns of TUG for these satellites, which closely match SVN 62 in Fig. 3. Furthermore, it may be noted that the affected set of satellites coincides with that for which only a partial set of calibration data is provided by Boeing (Sect. 2). As such, a problem in the manufacturer calibrations rather than a real anomaly of the respective antennas is suspected.

The consistency of manufacturer calibrations and observed patterns is described in Table 3. As may be seen, the manufacturer calibrations agree with the observed patterns of TU Graz at the 1–2 mm median RMS level. The most pronounced deviations are encountered for the IIR-A satellites, for which

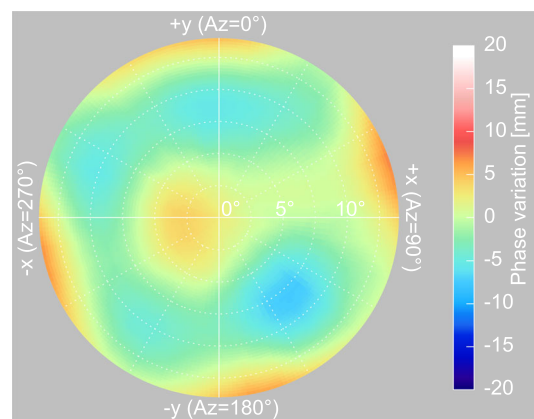


**Fig. 4** Boeing calibrations of SVN 65 L1/L2 phase patterns. Similar distortions show up in the calibrations of SVN 66 and 67

subtle differences may also be recognized in a visual comparison for other antenna types (Fig. 3). These hint at an impact of the spacecraft environment causing small but discernible changes of antenna patterns relative to the ground calibration after full integration of the antenna panel on the satellite. Such effects are commonly observed for GNSS receive antennas onboard low Earth orbit (LEO) satellites (Jäggi et al. 2009; Montenbruck et al. 2009), but have not been characterized and quantified for GNSS transmit antennas so far.

Comparing the azimuth- and block-averaged patterns currently employed in the IGS antenna model, with the full 2D patterns of TUG, median RMS differences close to 2 mm are encountered (Table 3). This is generally worse than the consistency of TUG and manufacturer calibrations, and indicates the benefit that can be expected from using satellite-specific



**Table 3** Block-specific statistics of GPS L1/L2 phase pattern differences between ground calibrated and observed patterns

Block	LMB–TUG	IGS–TUG
IIR-A	1.9	2.2
IIR-B/IIR-M	1.1	1.6
IIF	1.1	1.8
III	1.3	1.3

All values are given in mm and represent median values of the respective satellite-specific RMS differences on a triangular vertex grid. LMB = Lockheed Martin/Boeing

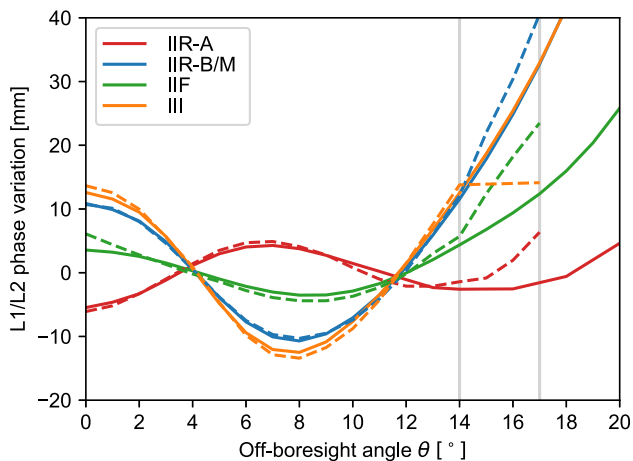


**Fig. 5** Block- and azimuth-averaged L1/L2 phase patterns from manufacturer calibrations (solid lines) and corresponding values of the igs20.atx antenna model (dashed lines). For proper comparison, a PCO and bias contribution has been removed from each data set based on equal weighting on a  $1^\circ$  grid up to  $14^\circ$  off-boresight angle. Gray lines mark the limits of the IGS model covered by Earth-based observations and the extension derived from LEO satellite measurements

2D transmit antenna phase patterns in precise GPS processing.

Despite the subtle deviations between ground calibrations and in-flight antenna characteristics, the manufacturer data offer unique advantages over the observed patterns. On the one hand, independent patterns are provided for each frequency band, which supports a consistent observation modeling in an uncombined processing scheme and facilitates a fully consistent use of triple-frequency (L1, L2, L5) observations. On the other hand, the ground calibrations cover an off-boresight angle of at least  $23^\circ$  and can seamlessly be applied for spaceborne platforms at altitudes of up to almost 10,000 km.

For illustration, Fig. 5 shows the variation of block- and azimuth-averaged phase patterns with off-boresight angle for the ionosphere-free L1/L2 combination. In accordance with the previous discussion, a good consistency of manufacturer calibrations and the IGS antenna model can be recognized over the range of off-boresight angles covered by observations with the IGS station network. Except for a 2.5 mm

difference in the IIF antenna pattern at  $\theta = 0^\circ$ , the agreement is always better than 1.1 mm. As may be recognized from the nonzero slope of the IIF phase variations in boresight direction, the discrepancy can readily be attributed to a deficiency of the IGS pattern estimates, which was first introduced into the igs08.atx antenna model and retained since then. Based on GPS tracking from LEO satellites with altitudes of up to 1340 km, extensions of the IIR-A, IIR-B/M, and IIF antenna patterns up to  $\theta = 17^\circ$  were derived in Jäggi et al. (2010) and Jäggi et al. (2012), which were subsequently adopted for the igs20.atx antenna model. For GPS III satellites, in contrast, no spaceborne observations were available when establishing the first IGS phase pattern model for these satellites, and a constant extension was adopted instead.

Improved extensions consistent with the other blocks were later presented in Conrad et al. (2023) and Dilssner et al. (2023), but have not been incorporated into the IGS antenna model so far. However, a very poor match of the IGS phase pattern extensions is also evident for IIR-A, IIR-B/M, and IIF satellites, which increases to roughly 10 mm at  $\theta = 17^\circ$ . This mismatch can primarily be attributed to the fact that the IGS values beyond  $\theta = 14^\circ$  do not represent absolute phase pattern, but have been determined relative to two Block IIA satellites. For these, a constant phase variation was arbitrarily assumed to allow for the separation of the unknown GPS transmit antenna patterns and LEO receive antenna phase patterns in that region (Jäggi et al. 2010, 2012). Among others, this results in a sudden change of slope of the IGS phase patterns at  $14^\circ$ , whereas the manufacturer calibrations exhibit a smooth variation with a continuous derivative at this point.

Due the fact that the patterns in Fig. 5 are minimized over the Earth coverage zone ( $\theta \leq 14^\circ$ ), a notable increase outside this region may be observed. This is most pronounced for the IIR-B/M and GPS III satellites, where values of 65 mm are attained at off-boresight angles of  $20^\circ$  for the azimuth-averaged L1/L2 patterns. In addition, notable azimuth variations may arise outside the Earth coverage zone of the transmit antennas. They are most pronounced for the IIR-A and IIF satellites and can attain amplitudes of about 10 mm level near  $\theta = 20^\circ$ . Evidently, use of azimuth-mean patterns is discouraged in this region and the use of 2D patterns is clearly advisable for the precise modeling of spaceborne GNSS observations beyond the common altitude range of current LEO missions.

## 4.2 Phase center offsets

For proper GNSS observation modeling, a consistent set of transmit antenna data is required, which comprises, on the one hand, the offset of the phase center from the center-of-mass and, on the other hand, the phase variations with respect to the phase center. Evidently, identical definitions of the phase center need to be applied for both parts of the



antenna model. Other than the Galileo antenna calibrations published in EUSPA (2022) and similar information for the Quasi-Zenith Satellite System (QZSS; Cabinet Office 2023), the presently available manufacturer calibrations of GPS IIR, IIR-M, IIF, and III antennas do, however, not satisfy this need and do not support a seamless use in GPS data analysis. All phase calibrations are referred to a block-specific calibration reference point, but no public information on the physical location of this point relative to the spacecraft body and COM has been disclosed. Likewise, no documentation is available for the phase center definition used in the determination of the PCOs released by NGA and Lockheed Martin.

Nevertheless, analysis of the phase calibration data (Fisher 2022) and independent PCOs for the GPS III satellites (Lockheed Martin 2021) provides strong evidence that phase centers derived by the manufacturers are adjusted by minimization of the phase variations using equal weighting and considering all measured grid points up to  $\theta_{\max} \approx 14^\circ$  (Sect. 2.3, Table 1). Based on this consideration, phase centers consistent with published PCOs can be estimated from the phase calibration data, and the CRP location can be inferred from comparison with the respective PCO values.

The individual  $z$ -components of the estimated CRP–COM offsets are illustrated in Fig. 6 for the various satellites and blocks based on numerical results summarized in Table 4. Block-mean values and their  $1\text{-}\sigma$  scatter amount to  $0.77 \pm 0.01$  m,  $0.91 \pm 0.04$  m,  $1.16 \pm 0.07$  m, and  $2.09 \pm 0.01$  m, respectively, for Block IIR-A, IIR-B/M, IIF, and GPS III satellites. The offsets correspond to roughly half the  $z$  body size of the individual spacecraft platforms, suggesting that the CRP is located close to the bottom of the antenna panel in all cases. In terms of scatter, notable differences may be observed among the various blocks, but it is not clear at this stage, whether the observed scatter reflects uncertainties in the quality of the phase center estimation or differences of COM location related to varying fuel mass or different payloads.

For IIR-B/M satellites, it is worth noting that the estimated CRP offsets can largely be divided into two groups with values of 0.85 m and 0.93 m. Within each of these groups, satellites show a better than 1 cm consistency of the CRP location with respect to the COM, but no final explanation for this grouping can be given at this stage. The largest scatter of the estimated CRP–COM offsets is encountered for the IIF satellites. Notably lower values than for the remaining satellites may be recognized for SVN 65–67. For these three satellites, no phase measurements from great-circle cuts have been released (Sect. 2) and the adjusted phase patterns show specific distortions that are not apparent for any of the other IIF satellites (Sect. 4.1). Both aspects raise concern about the quality of the antenna calibration for this group of satellites, but independent confirmation for this suspicion is currently not available.

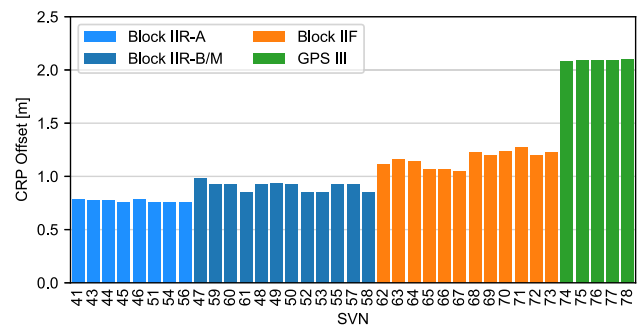


Fig. 6  $z$ -component of CRP–COM offset as derived from manufacturer calibrations of antenna phase variations and the L1 PCOs of NGA (Block IIR-A, IIR-B/M, and IIF) and Lockheed Martin (GPS III)

The L2 and L5 PCOs derived from the phase pattern calibrations and the NGA L1 PCOs are collated in Table 4 for the IIR-A, IIR-B/M, and IIF satellites. In the case of GPS III, the manufacturer-calibrated values are given for all three frequencies. Complementary to the frequency-specific PCOs, the corresponding values of the ionosphere-free L1/L2 and, where applicable, the L1/L5 combination are provided for comparison with IGS values and independent estimates.

For all GPS III satellites, the manufacturer PCOs exhibit a fixed offset of  $-89$  mm relative to the IGS value. It reflects the fact that the igs20.atx antenna model aims to retain the original PCOs of the Lockheed Martin factory calibrations to the extent possible, but applies a common 89 mm PCO shift for these satellites to align the estimated station heights in precise point positioning with the IGS20 reference frame. This frame is realized from GNSS observations, only, and aligned to the ITRF2020 scale at the 2015.0 reference epoch (Reischung et al. 2022; Altamimi et al. 2023). Differences between manufacturer-calibrated PCOs and IGS estimates obtained as part of the repro3 campaign exhibit a scatter of  $\pm 2$  cm across the five satellites available at the time (Reischung 2022). This is well below the observational uncertainty and provided good justification for use of the scale-adjusted manufacturer calibrations in the IGS antenna model.

An almost identical offset from igs20.atx is obtained for the GPS IIF satellites. Excluding the SVN 65–67 spacecraft, which were already mentioned for their suspicious phase patterns calibrations and anomalous PC–CRP offsets, a mean bias with respect to igs20.atx of 91 mm is found for the PCOs derived from the Boeing/NGA data. L1/L2 PCOs of individual IIF satellites exhibit a low scatter of about  $\pm 3$  cm. This suggests that the manufacturer-calibrated IIF PCOs are suitable candidates for incorporation into future updates of the IGS antenna model after conducting a block-specific scale alignment similar to GPS III.

Compared to GPS III and Block IIF, a less homogeneous picture is obtained for the IIR-B/M satellites. Most notably, SVN 49 and 55 stand out with increased negative or positive

**Table 4**  $z$ -components of calibration reference point and phase center offsets from center-of-mass for individual frequency bands and combinations derived from the manufacturer calibrations

SVN	Block	CRP	Manufacturer values					igs20.atx	Estimate	Difference
			L1	L2	L5	L1/L2	L1/L5	L1/L2	L1/L2	L1/L2
41	IIR-A	0.787	1.614	2.093		0.873	1.237	1.188	-0.049	
43	IIR-A	0.775	1.614	2.093		0.874	1.287	1.221	-0.066	
44	IIR-A	0.774	1.513	2.103		0.601	0.936	0.884	-0.052	
45	IIR-A	0.757	1.584	2.091		0.800	1.290	1.184	-0.106	
46	IIR-A	0.785	1.514	2.111		0.591	1.054	0.973	-0.081	
51	IIR-A	0.755	1.614	2.103		0.858	1.262	1.199	-0.063	
54	IIR-A	0.761	1.592	2.111		0.790	1.182	1.140	-0.042	
56	IIR-A	0.756	1.663	2.104		0.981	1.389	1.283	-0.106	
47	IIR-B	0.981	0.060	-0.395		0.763	0.771	0.759	-0.012	
59	IIR-B	0.921	-0.018	-0.485		0.704	0.719	0.697	-0.022	
60	IIR-B	0.925	0.000	-0.465		0.719	0.702	0.698	-0.004	
61	IIR-B	0.851	-0.082	-0.549		0.640	0.682	0.748	0.066	
48	IIR-M	0.923	0.001	-0.469		0.727	0.757	0.728	-0.029	
49	IIR-M	0.937	-0.023	-0.455		0.645	0.865	0.805	-0.060	
50	IIR-M	0.921	-0.017	-0.498		0.727	0.743	0.734	-0.009	
52	IIR-M	0.847	-0.058	-0.543		0.692	0.837	0.799	-0.038	
53	IIR-M	0.854	-0.101	-0.573		0.629	0.712	0.750	0.038	
55	IIR-M	0.929	-0.012	-0.455		0.672	0.576	0.593	0.017	
57	IIR-M	0.930	-0.015	-0.470		0.688	0.723	0.691	-0.032	
58	IIR-M	0.852	-0.094	-0.562		0.630	0.711	0.716	0.005	
62	IIF	1.113	1.093	0.924	0.801	1.354	1.461	1.454	1.487	0.033
63	IIF	1.161	1.091	0.921	0.812	1.354	1.443	1.421	1.455	0.034
64	IIF	1.140	1.090	0.902	0.786	1.381	1.474	1.462	1.516	0.054
65	IIF	1.063	1.093	0.913	0.832	1.371	1.422	1.352	1.412	0.060
66	IIF	1.070	1.090	0.890	0.847	1.400	1.397	1.436	1.442	0.006
67	IIF	1.052	1.092	0.887	0.877	1.409	1.363	1.411	1.470	0.059
68	IIF	1.222	1.092	0.895	0.853	1.397	1.393	1.460	1.493	0.033
69	IIF	1.201	1.091	0.887	0.796	1.406	1.463	1.482	1.522	0.040
70	IIF	1.234	1.084	0.892	0.829	1.381	1.406	1.472	1.516	0.044
71	IIF	1.273	1.093	0.922	0.821	1.357	1.436	1.434	1.426	-0.008
72	IIF	1.196	1.086	0.939	0.796	1.313	1.451	1.428	1.455	0.027
73	IIF	1.223	1.083	0.936	0.844	1.310	1.384	1.429	1.443	0.014
74	III	2.079	1.090	0.598	0.637	1.851	1.662	1.940	1.956	0.016
75	III	2.088	1.099	0.613	0.616	1.850	1.707	1.940	1.923	-0.017
76	III	2.087	1.094	0.618	0.636	1.831	1.672	1.920	1.946	0.026
77	III	2.094	1.098	0.612	0.595	1.850	1.733	1.939	1.963	0.024
78	III	2.096	1.096	0.592	0.600	1.876	1.722	1.965	1.995	0.030

L1 PCOs of IIR-A, IIR-B/M, and IIF satellites reflect the published values of NGA relative to which the L2 and L5 PCOs have been adjusted from the phase pattern calibrations. In the case of GPS III, the PCOs for all three frequency bands (L1, L2, and L5) represent manufacturer values. For comparison, values from the igs20.atx antenna model and new estimates (see Sect. 5) compatible with the manufacturer patterns and aligned to the IGS20 frame are given. All values in [m]

differences of the manufacturer-calibrated L1/L2 PCOs from the IGS values. For SVN 49, this is readily understood by the presence of satellite internal signal reflections after attaching an experimental signal payload to a spare input port of the antenna panel (Hauschild et al. 2012). The resulting multi-

path results in line-of-sight dependent group delay and phase variations that notably change the observed antenna pattern compared to the ground calibrations. Anomalous group delay variations have also been noted for SVN 55 by Springer and Dilssner (2009) and Wanninger et al. (2017), but presently

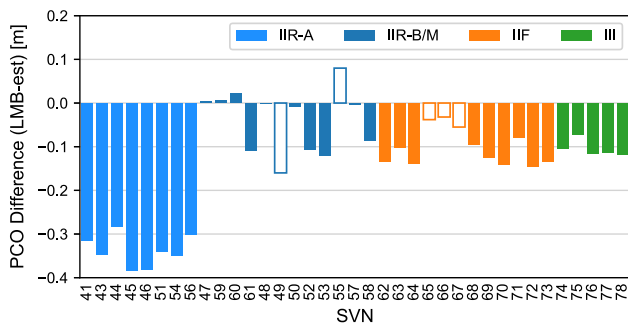


**Fig. 7**  $z$ -component of difference between manufacturer-calibrated L1/L2 PCOs and estimates based on the IGS20 reference frame. Empty bars indicate satellites with degraded or non-representative manufacturer calibrations

lack a technical explanation. Obviously, however, the pre-flight antenna calibrations of both satellites are no longer representative of the antenna characteristics after integration and cannot be considered as a viable alternative to the observation-based IGS antenna models.

L1/L2 PCOs of the remaining IIR-B/M satellites exhibit differences between +2 cm and -14 cm relative to the *igs20.atx* values. The corresponding mean value amounts to -44 mm, which is just half of the offset observed for IIF and GPS satellites. At the same time, the scatter across individual satellites is about 2–3 times larger than for the later satellite generations. It is presently unknown, whether the inhomogeneous results relate to uncertainties in the NGA PCOs, the Lockheed Martin phase calibrations, or satellite-specific changes of the antenna patterns after integration of the individual panels. In any case, use of the manufacturer-calibrated PCOs with a block-mean scale adjustment as used for IIF and GPS III cannot presently be recommended. However, use of the individual L1 and L2 PCOs may still be considered, when applying a satellite-specific correction in both frequency bands to align the resulting L1/L2 PCO to the observed IGS values. In this way, a consistent transition to frequency-specific antenna models may be supported without loosing consistency with established GNSS processing standards and existing geodetic time series.

Other than for the IIR-B/M, IIF, and GPS III satellites, a serious mismatch between manufacturer-based PCOs and the IGS antenna model may be noted for the Block IIR-A satellites. Here, a systematic bias of about -40 cm and a scatter of about ±10 cm across the satellites of this Block are encountered. It remains unclear, so far, whether this discrepancy relates to a misinterpretation of the NGA PCO values or a lower quality of the IIR-A calibrations, which were obtained in a different test facility than those of the modernized IIR-B/M antenna panels (Marquis and Reigh 2015). In any case, satellite-specific rather than block-specific corrections would need to be applied to the manufacturer PCOs for incorporation into a future IGS antenna model.

## 5 IGS20-aligned Lockheed Martin and Boeing antenna model

As discussed above, manufacturer-calibrated GPS antenna data can offer a valuable enhancement of the present IGS antenna model. However, care needs to be taken to align the manufacturer calibrations with the scale of the IGS20 reference frame to preserve consistency with established processing standards and geodetic time series. Even though the comparison of manufacturer-calibrated PCOs with IGS values in Sect. 4.2 provides a basic insight into the consistency (or non-consistency) of the respective data sets for individual blocks of GPS satellites, the obtained differences cannot be used directly to align the manufacturer PCOs with the *igs20.atx* model. This is due to the fact that manufacturer-calibrated PCOs and *igs20.atx* PCOs are to be used with distinct sets of phase patterns that make use of different, and partly incompatible, phase center conventions.

For full consistency, PCOs compatible with the IGS20 reference frame have therefore been determined in the present study based on the manufacturer-calibrated phase patterns (see Sect. 4.1). The estimation is based on 6.5 years of data (January 2017–June 2023) to cover all satellites of the Block IIR-A, IIR-B/M, IIF, and GPS III generations. GPS observations from 120–150 stations of the IGS network (IGS 2023) were processed in daily batches with the NAPEOS software (Springer 2009) for a global adjustment of satellite, station, atmospheric, and Earth rotation parameters. Station coordinates were tightly constrained to a priori values from the IGS20 reference frame (Rebischung et al. 2022) to allow for the estimation of IGS20-compatible phase center offsets of the individual GPS satellites.

Use of the manufacturer-calibrated phase patterns instead of the azimuth-averaged *igs20.atx* pattern introduces moderate changes at the level of few to at most 10 cm in the estimated PCOs of individual satellites (Table 4). The resulting differences between the manufacturer calibrations and the newly derived PCO estimates are illustrated in Fig. 7. Aside from slightly modified values of the block-specific differences between calibrated and estimated PCOs, the results are in full agreement with the initial analysis of Sect. 4.2. In particular, they support the suggested use of block-mean corrections for both the GPS III satellites and the nine trustworthy Block IIF satellites to adjust the manufacturer PCOs to the IGS20 reference frame. The respective block-mean differences amount to -12.2 cm (IIF) and -10.5 cm (III), which differ slightly from the values discussed Sect. 4.2, but reflect the use of different phase patterns in *igs20.atx* and in the present PCO estimation. PCO differences of individual satellites exhibit a 1- $\sigma$  scatter of 2.5 cm for Block IIF and 1.8 cm for GPS III satellites.

For the IIR-B/M satellites, one may note two obvious groups: while six satellites show a near perfect consistency

of calibrated and estimated PCOs, the other group (SVN 61, 52, 53, 58) shows a difference of about  $-10\text{ cm}$  that is well consistent with the IIF and GPS III satellites. In the absence of more detailed spacecraft information, it remains unclear, though, whether this finding relates to undocumented differences in the center-of-mass or antenna position or modifications of the antenna characteristics following satellite integration. In the case of the Block IIR-A satellites, PCO differences between manufacturer calibrations and the new estimates are slightly smaller in magnitude ( $34\text{ cm}$  vs.  $41\text{ cm}$ ) than for the *igs20.atx* PCOs, but still much larger than tolerable for use of the manufacturer PCOs in practical GNSS data processing. Overall, block-mean PCO corrections do not appear justified for incorporation of Block IIR-A as well as IIR-B and IIR-M antenna calibrations into a new antenna model. Instead, satellite-specific PCO corrections appear best suited to benefit from frequency-specific manufacturer calibrations for these satellites, while retaining compatibility with the IGS20 reference frame scale.

Building up on the above considerations and analysis results, a new *lmb20.atx* antenna model for GPS IIR-A/B/M, IIF, and III satellites has been prepared that best exploits the benefits of the Lockheed Martin and Boeing (LMB) calibrations but is aligned to the current IGS frame realization. It includes azimuth and off-boresight angle dependent phase patterns for each transmitted frequency that are derived from the manufacturer calibration by minimization over a rectangular grid with nominal  $2^\circ$  sampling in off-boresight angle up to  $\theta = 14^\circ$  (or  $14.3^\circ$  for IIF satellites). Suspicious patterns for SVN 65–67 are replaced by block-mean patterns of the remaining IIF satellites. A block-mean pattern is also used for SVN 79, for which no calibrations have been published so far. For use in LEO satellite applications, the phase patterns include data up to  $\theta = 20^\circ$ , which exceeds the current  $17^\circ$  limit of the *igs20.atx* antenna model and covers an altitude regime up to  $2700\text{ km}$ .

Frequency-specific phase center offsets from the center-of-mass are derived through combination of the antenna phase calibration data with NGA L1 PCOs for the IIR-A/B/M and IIF satellites while GPS III PCOs are given by Lockheed Martin (Table 4). For alignment with the IGS20 reference frame scale, a common correction is then applied to the L1, L2, and, optionally L5 PCOs based on the difference between the calibrated and observed L1/L2 PCOs. A machine-readable version of the resulting *lmb20.atx* antenna model in ANTEX v1.4 antenna exchange format (Rothacher and Schmid 2010) is made available for public use as an electronic supplement to the present article. It enables community testing of the manufacturer-calibrated GPS antenna patterns and may serve as a prototype for a future enhancement of the IGS antenna model.

## 6 Summary and conclusions

With the recent release of antenna calibrations for the GPS Block IIF satellites, manufacturer calibrations are now available for all types of satellites in the current GPS constellation. Using plausible assumptions on the conceptual definition of the antenna phase centers and the nature of published phase center offsets from independent sources, the phase variations can be reduced to a consistent phase center, thus giving a combined set of PCOs and PHVs for each individual frequency.

The manufacturer-calibrated phase variations of Block IIR, IIR-M, IIF, and GPS III satellites exhibit good consistency of the PCO-free phase variations with the azimuth-averaged values in the IGS antenna model and azimuth-dependent phase pattern estimates of TUG determined for this study. We therefore recommend to include these calibrations into future releases of the IGS antenna model. Compared to the currently available IGS patterns, use of the manufacturer calibrations promises improved precision in the observation modeling by properly accounting for both the boresight angle variation and the azimuth dependence. Furthermore, the availability of manufacturer calibrations for the individual frequency bands overcomes the limitations of pattern estimates based on ionosphere-free dual-frequency combinations. It therefore paves the way for a consistent multi-frequency processing using uncombined observations (Schönemann et al. 2011; Odijk et al. 2016; Zhou et al. 2018; Strasser et al. 2019). Finally, use of the manufacturer calibrations enables a seamless extension to off-boresight angles beyond  $14^\circ$  that are required for processing of spaceborne GPS observations (Conrad et al. 2023).

The manufacturer-calibrated PCOs exhibit a varying level of consistency with the independent estimates from global GNSS monitoring networks. Compared to PCO estimates compatible with the scale of the ITRF2020 and IGS20 reference frame, the pre-flight calibrations of the Block IIF and GPS III satellites exhibit block-mean differences of  $12.2\text{ cm}$  and  $10.5\text{ cm}$ , respectively, with a scatter of  $\sigma \approx 2\text{ cm}$  across individual satellites. The mean PCO offset translates into station height differences of  $5\text{--}6\text{ mm}$  and thus a TRF scale offset of  $0.8\text{--}1.0\text{ ppb}$  (Montenbruck et al. 2022). Considering the different orbit height, the GPS IIF/III PCO biases correspond closely to the offset of Galileo manufacturer calibrations from IGS20-aligned PCO estimates (Steigenberger and Montenbruck 2023) and the  $15.5\text{ cm}$  correction applied in the *igs20.atx* model to align the Galileo PCO calibrations in EUSPA (2022) with the IGS20 reference frame scale (Reischung et al. 2022). Even though an inferior consistency is obtained for the Block IIR-B/IIR-M PCOs and, most notably the IIR-A calibrations, the results suggest a need to carefully revisit the contribution and possible benefit of GNSS for the definition of the ITRF scale.



On the other hand, it is obvious that the definition of a GNSS-based reference frame scale based on manufacturer calibrations of the transmit antennas depends largely on the availability of fully consistent phase center and pattern information. This condition is readily met by the publicly released Galileo antenna data, but has, unfortunately, not received proper attention in the compilation of the respective GPS calibrations. So far, an undue set of assumptions are required to mate the phase calibrations, which refer to an unknown calibration reference point, with phase center offsets relative to the spacecraft center-of-mass. This is most critical for the IIR-A, IIR-B/M, and IIF satellites, where NGA PCOs need to be used that lack a proper traceability and documentation. However, it likewise applies for GPS III, where the concise phase center definition remains undocumented and has to be inferred through reverse engineering.

The GPS provider and satellite manufacturers are therefore strongly encouraged to publish missing information on the location of the calibration reference points relative to the spacecraft center-of-mass. This would clearly foster a comprehensive incorporation of the manufacturer calibrations into antenna models for precise GPS data processing and make them fully competitive with the respective antenna calibration data released by the Galileo project.

**Supplementary Information** The online version contains supplementary material available at <https://doi.org/10.1007/s00190-023-01809-y>.

**Acknowledgements** The public release of transmit antenna calibrations through the GPS project and the satellite manufacturers (Lockheed Martin and Boeing) is gratefully acknowledged. This study makes use of GPS observations collected by the global receiver network of the International GNSS Service (IGS). The work of all station operators and data centers is likewise acknowledged. The NAPEOS software used in this study is operated under license of the European Space Agency.

**Author Contributions** OM proposed the idea of the study, processed the raw calibration data, and formulated the draft manuscript. PS and TMG contributed estimates of phase center offsets and patterns based on the analysis of GPS observations from a global station network. All authors contributed to the discussion of results and critically reviewed the final version of the manuscript.

**Funding** Open Access funding enabled and organized by Projekt DEAL.

**Data availability** Raw antenna calibration data of Lockheed Martin and Boeing are publicly available through the Navigation Center of the US Coast Guard (<https://www.navcen.uscg.gov/gps-technical-references>). IGS antenna models are provided at <https://files.igs.org/pub/station/general/>. GPS observation data from the IGS network are publicly available through the IGS and its data centers such as CDDIS <https://cddis.nasa.gov/archive/gnss/data/>. The lmb20.atx antenna model developed in the present study is made available in ANTEX v1.4 format as an electronic supplement of this article.

## Declarations

**Conflict of interest** The authors have no conflicts of interest that are relevant to the content of this article.

**Open Access** This article is licensed under a Creative Commons Attribution 4.0 International License, which permits use, sharing, adaptation, distribution and reproduction in any medium or format, as long as you give appropriate credit to the original author(s) and the source, provide a link to the Creative Commons licence, and indicate if changes were made. The images or other third party material in this article are included in the article's Creative Commons licence, unless indicated otherwise in a credit line to the material. If material is not included in the article's Creative Commons licence and your intended use is not permitted by statutory regulation or exceeds the permitted use, you will need to obtain permission directly from the copyright holder. To view a copy of this licence, visit <http://creativecommons.org/licenses/by/4.0/>.

## References

- Altamimi Z, Rebischung P, Collilieux X, Métivier L, Chanard K (2023) ITRF2020: an augmented reference frame refining the modeling of nonlinear station motions. *J Geodesy* 97(5):47. <https://doi.org/10.1007/s00190-023-01738-w>
- Bar-Sever Y, Bertiger W, Byun S, Desai S, Haines B, Hajj G (2006) Calibrating the GPS satellites transmit antenna. In: IGS Workshop 2006, [https://files.igs.org/pub/resource/pubs/06\\_darmstadt/IGS%20Presentations%20PDF/10\\_5\\_Bar-Sever.pdf](https://files.igs.org/pub/resource/pubs/06_darmstadt/IGS%20Presentations%20PDF/10_5_Bar-Sever.pdf)
- Cabinet Office (2023) QZSS satellite information, Oct. 31, 2023. <https://qzss.go.jp/en/technical/qzssinfo/index.html>
- Conrad A, Desai S, Haines B, Axelrad P (2023) Extending the GPS IIIA antenna calibration for precise orbit determination of low Earth orbit satellites. *J Geodesy* 97(4):35. <https://doi.org/10.1007/s00190-023-01718-0>
- Dilssner F (2010) GPS IIF-1 satellite antenna phase center and attitude modeling. *Inside GNSS* 5(6):59–64
- Dilssner F, Springer T, Schönemann E, Enderle W (2016) Evaluating the pre-flight GPS Block IIR/IIR-M antenna phase pattern measurements. In: IGS Workshop 2016, <https://files.igs.org/pub/resource/pubs/workshop/2016/W2016%20-%20PY0704%20-%20Dilssner.pdf>
- Dilssner F, Springer T, Schönemann E, Gini F, Enderle W (2023) New type on the block: generating high-precision orbits for GPS III satellites. *GPS World* 34(5):44–49
- EUSPA (2022) Galileo satellite metadata, European Global Navigation Satellite Systems Agency. <https://www.gsc-europa.eu/support-to-developers/galileo-satellite-metadata>
- Fisher A (2022) GPS III Earth coverage (EC) antenna patterns – SV-specific patterns: plots, directivity, phase; Lockheed Martin Space; May 2022. [https://www.navcen.uscg.gov/sites/default/files/pdf/gps/GPS\\_ZIP/GPS\\_III\\_EC\\_Antenna\\_Patterns\\_SVN\\_74\\_75\\_76\\_77\\_78.pdf](https://www.navcen.uscg.gov/sites/default/files/pdf/gps/GPS_ZIP/GPS_III_EC_Antenna_Patterns_SVN_74_75_76_77_78.pdf)
- Hartman T, Boyd LR, Koster D, Rajan JA, Harvey J (2000) Modernizing the GPS Block IIR spacecraft. *Proceedings of ION GPS 2000*, pp. 2115–2121
- Hauschild A (2017) Basic observation equations. In: Teunissen P, Montenbruck O (eds) *Springer Handbook of Global Navigation Satellite Systems*, Chapter 19. Springer, Cham, pp 561–582. [https://doi.org/10.1007/978-3-319-42928-1\\_19](https://doi.org/10.1007/978-3-319-42928-1_19)
- Hauschild A, Montenbruck O, Thöler S, Erker S, Meurer M, Ashjaee J (2012) A multi-technique approach for characterizing the SVN49 signal anomaly, part 1: receiver tracking and IQ constellation. *GPS Solut* 16(1):19–28. <https://doi.org/10.1007/s10291-011-0203-2>

- IGS (2023) Daily 30-second Hatanaka-compressed observation data. Int GNSS Service (IGS). [https://doi.org/10.5067/GNSS/gnss\\_daily\\_d\\_001](https://doi.org/10.5067/GNSS/gnss_daily_d_001)
- Igwe C (2023) GPS-IIF satellites: antenna patterns for L1, L2 and L5 (SVN 62–73). <https://www.navcen.uscg.gov/gps-technical-references>
- Jäggi A, Dach R, Montenbruck O, Hugentobler U, Bock H, Beutler G (2009) Phase center modeling for LEO GPS receiver antennas and its impact on precise orbit determination. *J Geodesy* 83(12):1145–1162. <https://doi.org/10.1007/s00190-009-0333-2>
- Jäggi A, Dach R, Bock H, Beutler G, Montenbruck O, Schmid R (2010) Extending the GPS satellite antenna patterns of the IGS to nadir angles beyond 14° using LEO data. In: AGU Fall Meeting, G54A-06, [http://www.bernese.unibe.ch/publist/2010/pres/aj\\_agu2010\\_17Dec.pdf](http://www.bernese.unibe.ch/publist/2010/pres/aj_agu2010_17Dec.pdf)
- Jäggi A, Dilssner F, Schmid R, Dach R, Springer T, Bock H, Steigenberger P, Lutz S (2012) Extension of the GPS satellite antenna patterns to nadir angles beyond 14°. In: IGS Workshop 2012, Olsztyn, Poland, <https://files.igs.org/pub/resource/pubs/workshop/2012/Poland%202012%20-%20P09%20Dach%20PR14.pdf>
- Johnston G, Riddell A, Hausler G (2017) The International GNSS Service. In: Teunissen P, Montenbruck O (eds) Springer Handbook of Global Navigation Satellite Systems, Chapter 33. Springer, Cham, pp 967–982. [https://doi.org/10.1007/978-3-319-42928-1\\_33](https://doi.org/10.1007/978-3-319-42928-1_33)
- Kenner H (2003) Geodesic math and how to use it. Univ of California Press, Berkeley
- Lockheed Martin (2019) Phase center offsets, group delay and inter-signal correction values for SVN-74, January 2019. [https://www.navcen.uscg.gov/sites/default/files/pdf/gps/SVN74\\_APC\\_ISC\\_data\\_release\\_Jan2019.pdf](https://www.navcen.uscg.gov/sites/default/files/pdf/gps/SVN74_APC_ISC_data_release_Jan2019.pdf)
- Lockheed Martin (2021) Updated GPS-III antenna phase center values for SVN-74 through SVN-78 and timing group delay and inter-signal correction values as measured at the factory for SVN-78, December 2021. [https://www.navcen.uscg.gov/sites/default/files/pdf/gps/GPSIII\\_APCs\\_SVNs\\_74\\_78\\_ISC\\_SVN78\\_Dec2021.pdf](https://www.navcen.uscg.gov/sites/default/files/pdf/gps/GPSIII_APCs_SVNs_74_78_ISC_SVN78_Dec2021.pdf)
- Malys S, Solomon R, Drotar J, Kawakami T, Johnson T (2021) Compatibility of terrestrial reference frames used in GNSS broadcast messages during an 8-week period of 2019. *Adv Space Res* 67(2):834–844. <https://doi.org/10.1016/j.asr.2020.11.029>
- Maqsood M, Gao S, Montenbruck O (2017) Antennas. In: Teunissen P, Montenbruck O (eds) Springer Handbook of Global Navigation Satellite Systems. Chapter 17 Springer, Cham, pp 505–534. [https://doi.org/10.1007/978-3-319-42928-1\\_17](https://doi.org/10.1007/978-3-319-42928-1_17)
- Marquis W (2014) The GPS Block IIR/IIR-M antenna panel pattern; Appendix C - IIR and IIR-M SV-specific patterns, phase data. Lockheed Martin Space Systems Company. <https://www.navcen.uscg.gov/sites/default/files/ppt/gps/AppCAntennaPanelPatterns.pptx>
- Marquis W (2015) The GPS Block IIR/IIR-M antenna panel pattern, revision May 2015. Lockheed Martin Space Systems Company. [https://navcen.uscg.gov/sites/default/files/pdf/gps/GPS\\_Block\\_IIR\\_IIR\\_M\\_Antenna\\_Panel\\_Pattern\\_Marquis\\_Aug2015\\_revised.pdf](https://navcen.uscg.gov/sites/default/files/pdf/gps/GPS_Block_IIR_IIR_M_Antenna_Panel_Pattern_Marquis_Aug2015_revised.pdf)
- Marquis W (2016) The GPS Block IIR antenna panel pattern and its use on-orbit. In: Proceedings of ION GNSS+ 2016, pp 2896–2909. <https://doi.org/10.33012/2016.14596>
- Marquis WA, Reigh DL (2015) The GPS Block IIR and IIR-M broadcast L-band antenna panel: its pattern and performance. *NAVIGATION J Instit Navigat* 62(4):329–347. <https://doi.org/10.1002/navi.123>
- Martzen P, Highsmith D, Valdez J, Parker J, Moreau M (2015) GPS antenna characterization experiment (ACE): receiver design and initial results. In: Proceedings of ION Joint Navigation Conference
- Mayer-Gürr T, Behzadpour S, Eicker A, Ellmer M, Koch B, Krauss S, Pock C, Rieser D, Strasser S, Süsner-Rechberger B et al (2021) GROOPS: a software toolkit for gravity field recovery and GNSS processing. *Comput Geosci* 155(104):864. <https://doi.org/10.1016/j.cageo.2021.104864>
- Montenbruck O, Garcia-Fernandez M, Yoon Y, Schön S, Jäggi A (2009) Antenna phase center calibration for precise positioning of LEO satellites. *GPS Solut* 13(1):23–34. <https://doi.org/10.1007/s10291-008-0094-z>
- Montenbruck O, Schmid R, Mercier F, Steigenberger P, Noll C, Fatkulin R, Kogure S, Ganeshan AS (2015) GNSS satellite geometry and attitude models. *Adv Space Res* 56(6):1015–1029. <https://doi.org/10.1016/j.asr.2015.06.019>
- Montenbruck O, Steigenberger P, Villiger A, Rebischung P (2022) On the relation of GNSS phase center offsets and the terrestrial reference frame scale: a semi-analytical analysis. *J Geodesy* 96(11):90. <https://doi.org/10.1007/s00190-022-01678-x>
- NGA (2014) NGA GPS ephemeris/station/antenna offset documentation; effective date November 1, 2014. [https://web.archive.org/web/20141128063431/http://earth-info.nga.mil:80/GandG/sathtml/gpsdoc2014\\_11a.html](https://web.archive.org/web/20141128063431/http://earth-info.nga.mil:80/GandG/sathtml/gpsdoc2014_11a.html)
- NGA (2020) NGA GNSS division precise ephemeris parameters; February 20, 2020. <https://earth-info.nga.mil/php/download.php?file=gnss-precise>
- NGA (2021) Recent update to WGS 84 reference frame and NGA transition to IGS ANTEX. [https://earth-info.nga.mil/php/download.php?file=\(U\)WGS%2084\(G2139\).pdf](https://earth-info.nga.mil/php/download.php?file=(U)WGS%2084(G2139).pdf)
- Odijk D, Zhang B, Khodabandeh A, Odolinski R, Teunissen PJ (2016) On the estimability of parameters in undifferenced, uncombined GNSS network and PPP-RTK user models by means of S-system theory. *J Geodesy* 90(1):15–44. <https://doi.org/10.1007/s00190-015-0854-9>
- Rebischung P (2022) IGS repro3: Terrestrial frame combination outcomes. In: IGS Virtual Workshop, 30 June 2022, [https://files.igs.org/pub/resource/pubs/workshop/2022/IGSW2022\\_S12\\_01\\_Rebischung.pdf](https://files.igs.org/pub/resource/pubs/workshop/2022/IGSW2022_S12_01_Rebischung.pdf)
- Rebischung P, Schmid R (2016) IGS14/igs14.atx: a new framework for the IGS products. In: AGU Fall Meeting, G41A-0998
- Rebischung P, Villiger A, Masoumi S, Herring T (2022) Upcoming switch to IGS20/igs20.atx and repro3 standards, IGSMAIL-8238. <https://lists.igs.org/pipermail/igsmail/2022/008234.html>
- Rothacher M, Schmid R (2010) ANTEX: The antenna exchange format, version 1.4, 10 September 2010. <https://files.igs.org/pub/data/format/antex14.txt>
- Schmid R, Rothacher M, Thaller D, Steigenberger P (2005) Absolute phase center corrections of satellite and receiver antennas: impact on global GPS solutions and estimation of azimuthal phase center variations of the satellite antenna. *GPS Solut* 9(4):283–293. <https://doi.org/10.1007/s10291-005-0134-x>
- Schmid R, Dach R, Collilieux X, Jäggi A, Schmitz M, Dilssner F (2016) Absolute IGS antenna phase center model igs08.atx: status and potential improvements. *J Geodesy* 90(4):343–364. <https://doi.org/10.1007/s00190-015-0876-3>
- Schönemann E, Becker M, Springer T (2011) A new approach for GNSS analysis in a multi-GNSS and multi-signal environment. *J Geodetic Sci* 1(3):204–214. <https://doi.org/10.2478/v10156-010-0023-2>
- Springer T, Dilssner F (2009) SVN49 and other GPS anomalies. *Inside GNSS* 4(4):32–36
- Springer TA (2009) NAPEOS mathematical models and algorithms, DOPS-SYS-TN-0100-OPS-GN. ESA/ESOC, Darmstadt
- Steigenberger P, Montenbruck O (2023) Consistency of Galileo satellite antenna phase center offsets. *J Geodesy* 97(6):58. <https://doi.org/10.1007/s00190-023-01750-0>
- Steigenberger P, Thaelert S, Montenbruck O (2020) GPS III Vespucci: results of half a year in orbit. *Adv Space Res* 66(12):2773–2785. <https://doi.org/10.1016/j.asr.2020.03.026>
- Strasser S, Mayer-Gürr T, Zehentner N (2019) Processing of GNSS constellations and ground station networks using the raw obser-

- vation approach. *J Geodesy* 93(7):1045–1057. <https://doi.org/10.1007/s00190-018-1223-2>
- Thoelert S, Steigenberger P, Montenbruck O, Meurer M (2019) Signal analysis of the first GPS III satellite. *GPS Solut* 23(4):92. <https://doi.org/10.1007/s10291-019-0882-7>
- Villiger A (2022) Upcoming switch to IGS20/igs20.atx and repro3 standards, IGSMail-8238. <https://lists.igs.org/pipermail/igsmail/2022/008234.html>
- Wanninger L, Sumaya H, Beer S (2017) Group delay variations of GPS transmitting and receiving antennas. *J Geodesy* 91(9):1099–1116. <https://doi.org/10.1007/s00190-017-1012-3>
- Wu JT, Wu SC, Hajj G, Bertiger WI, Lichten SM (1993) Effects of antenna orientation on GPS carrier phase. *Manuscripta Geodaetica* 18(2):91–98
- Zehentner N (2016) Kinematic orbit positioning applying the raw observation approach to observe time variable gravity. PhD thesis, Graz University of Technology
- Zhou F, Dong D, Li W, Jiang X, Wickert J, Schuh H (2018) GAMP: an open-source software of multi-GNSS precise point positioning using undifferenced and uncombined observations. *GPS Solut* 22(2):33. <https://doi.org/10.1007/s10291-018-0699-9>
- Zhu S, Massmann FH, Yu Y, Reigber C (2003) Satellite antenna phase center offsets and scale errors in GPS solutions. *J Geodesy* 76(11):668–672. <https://doi.org/10.1007/s00190-002-0294-1>